

Theoretical and experimental study of the adsorption characteristics of Methylene Blue on titanium dioxide surface using DFT and Monte Carlo dynamic simulation

Malika Khnifira^a, Sana El Hamidi^a, Aicha Machrouhi^a, Anass Mahsoune^a, Wafaa Boumya^a, Hanane Tounsadi^{a,b}, Fatima Zahra Mahjoubi^{a,c,*}, Mhamed Sadiq^a, Nouredine Barka^a, Mohamed Abdennouri^a

^aSultan Moulay Slimane University of Beni Mellal, Research Group in Environmental Sciences and Applied Materials (SEMA), FP Houribga, B.P. 145, 25000 Houribga, Morocco, email: mahjoubi.fatimazahra@gmail.com (F.Z. Mahjoubi), Tel. +212652846635; email: khniframalak2014@gmail.com (M. Khnifina), Tel. +212606403888; email: sanaa.elhamidi@gmail.com (S. El Hamidi), Tel. +212 651039586; email: machrouhi.aicha90@gmail.com (A. Machrouhi), Tel. +212 651112705; email: anassmahsoune@gmail.com (A. Mahsoune), Tel. +212 661 66 66 22; email: wafaa-angel@hotmail.fr (W. Boumya), Tel. +212645208564; email: hananetounsadi@gmail.com (H. Tounsadi), Tel. +212 666248196; email: sadiqmhamed@hotmail.com (M. Sadiq), Tel. +212 661 66 66 22; email: barkanouredine@yahoo.fr (N. Barka), Tel. +212667669039; email: abdenmourimohamed@yahoo.fr (M. Abdennouri)

^bLaboratoire d'Ingénierie, d'Electrochimie, Faculté des Sciences Dhar Elmehraz, de Modélisation et d'Environnement (LIEME), Université Sidi Mohamed Ben Abdellah, Fès, Morocco

^cLaboratory of Spectro-Applied Chemometric and Environment (LSCAE), University Sultan Moulay Slimane, FST Beni Mellal, B.P. 523, Béni-Mellal, Morocco

Received 25 September 2019; Accepted 14 February 2020

ABSTRACT

In the present work, the experimental and theoretical studies of the adsorption of methylene blue (MB) on TiO₂ were established. The geometry of MB was optimized by density functional theory (DFT) at the B3LYP/LanL2DZ level of theory using Gaussian software 09W, then after, the adsorption on anatase (110) TiO₂ surface in aqueous solution was carried out by Monte Carlo dynamic simulation. Theoretical results show that the fully protonated MB in the three nitrogen atoms has a high negative PA which indicates their better tendency of chemical adsorption to TiO₂ surface than neutral or partially protonated. Then, quantum chemical parameters, electronic distribution, total, average total, intermolecular, electrostatic, and van der Waals energies for the systems were evaluated and interpreted. According to the results, MB was chemisorbed in each case of neutral and protonated species. A systematic study of various parameters (amount of TiO₂, contact time, initial concentration, temperature, pH), was performed. Experimental results show that the adsorption was rapid and was best fitted with the pseudo-second-order kinetic model instead of pseudo-first-order kinetic and Elovich models. The values of thermodynamic parameters ΔG° , ΔS° , and ΔH° indicate that the adsorption was spontaneous and exothermic in nature. The adsorption follows the Langmuir isotherm model in agreement with quantum chemical parameters obtained by DFT and MCDS.

Keywords: Methylene Blue; Adsorption; TiO₂ (110) anatase; Langmuir isotherm; MCDS; DFT

* Corresponding author.

1. Introduction

Discharging large quantities of dyes in water resources from various dyestuff manufactures, paper making industries textile, and plastic pose many hazardous environmental problems. Furthermore, the majority of dye molecules are composed of aromatic rings, rendering them carcinogenic and mutagenic for aquatic organisms [1]. The organic molecules, especially methylene blue (MB) contained in the wastewater are hardly biodegradable and the lack or insufficiency of treatment systems thus leads to their accumulations in the water cycle [2]. To reduce the harmful effects of this pollutant, several methods of wastewater treatment were tested such as membrane filtration, solvent extraction, electrochemical methods, chemical precipitation, adsorption, biological methods, and catalytic oxidation. Among these techniques, the adsorption process appears as a method of choice because of its easy operation, flexibility, simplicity in design, and insensitivity towards the pollutants as well as toxic compounds [3–6].

Many adsorbents such as carbon nanotubes, activated carbon, bentonite, ash, coal, manganese oxides, almond shell, kaolinite, bagasse, clay, phosphate, zeolite, resins, compost, and titan dioxide, that is, have been applied for the adsorption of dyes in aqueous environments [7,8]. Activated carbon (AC) is widely used as an effective adsorbent in the removal of dyes and it is proven to be an effective adsorbent for the removal of a variety of organic and inorganic pollutants dissolved in aqueous media or from the gaseous environment. But, many disadvantages are associated with this adsorbent including high cost, non-renewable production source and difficulties with its regeneration reuse give a reduction in adsorptive efficiency [3]. In this study, we choose TiO_2 as an adsorbent because it is easy to synthesize and has a rigid structure allowing us to study the adsorption at a molecular dynamic scale. Moreover, TiO_2 electronic properties, low economic cost, chemical stability, and non-toxicity make it an excellent adsorbent. In recent years, several studies showed a good photocatalytic performance of TiO_2 in the degradation of organic substrates [9–12].

Most of the organic molecules containing the heteroatoms ($=\text{N}-$, $-\text{O}-$, $-\text{S}-\text{Cl}$) and several bonds facilitate their adsorption on TiO_2 surface [13]. So, understanding the interaction of organic molecules with the TiO_2 surface is important for several types of research in technological applications, including photocatalysis [14] and dye-sensitized solar cells [15].

The important adsorption process is then controlled by the strength of the molecular interactions with the adsorbent surface. The current understanding of the interactions of organic molecules with TiO_2 surfaces has been summarized in a recent review by Thomas and Syres [16]. Because of its scientific and practical importance, the adsorption of organic molecules is one of the most developing areas of research in the field of titanium oxide surface science.

This study aimed to understand the adsorption process of methylene blue on the TiO_2 (110) anatase surface by Monte Carlo dynamic simulation (MCDS). Experimental and theoretically studies of the interaction of neutral and protonated forms of MB dye with TiO_2 surfaces in the presence of water molecules were established. Density functional theory (DFT) calculations at the B3LYP/LanL2DZ level were used

to understand the electronic properties of these forms based on the natural bond orbital analysis (NBO). MCDS was used to estimate the relative adsorption strengths for different sites. The adsorption geometries and energies for different configurations were also obtained in the simulation box for comparison.

On the other hand, an experimental study was realized to evaluate the effect of certain individual parameters on adsorption of MB by TiO_2 such as pH, temperature, dye concentration and the mass of TiO_2 . The chemical structure of the MB is illustrated in Fig. 1.

2. Theoretical study

2.1. Methods

2.1.1. DFT calculation

Gaussian 09W program was used for the calculations. All the geometries of the MB forms were optimized using B3LYP/LANL2DZ basis set. The electronic properties of these structures were studied based on the NBO analysis. The most popular parameters which play a prominent role are involved in chemical reactivity. These involve the eigenvalues of the energy of the highest occupied molecular orbital (E_{HOMO}), energy of the lowest occupied molecular orbital (E_{LUMO}), energy gap (ΔE_{gap}), ionization energy (IE), electron affinity (EA), absolute electronegativity (χ), global hardness (η), global softness (S), global electrophilicity index (ω), fraction of electrons transferred (ΔN) [17].

$$\text{IE} = -E_{\text{HOMO}} \quad (1)$$

$$\text{EA} = -E_{\text{LUMO}} \quad (2)$$

The gap energy (Eq. (3)) is the difference between the energy of the lowest unoccupied molecular orbital (E_{LUMO}) and the energy of the highest occupied molecular orbital (E_{HOMO}).

$$\Delta E_{\text{gap}} (\text{eV}) = E_{\text{LUMO}} - E_{\text{HOMO}} \quad (3)$$

The absolute chemical hardness (Eq. (4)) was calculated according to the equation.

$$\eta = \frac{I - A}{2} = \frac{E_{\text{LUMO}} - E_{\text{HOMO}}}{2} \quad (4)$$

The chemical softness, which describes the ability of an atom or a group of atoms to accept electrons, as shown in Eq. (5).

$$S = \frac{1}{\eta} = \frac{2}{E_{\text{HOMO}} - E_{\text{LUMO}}} \quad (5)$$

The electronegativity of coating behavior was calculated according to Eq. (6).

$$\chi = \frac{I + A}{2} = \frac{-(E_{\text{LUMO}} - E_{\text{HOMO}})}{2} \quad (6)$$

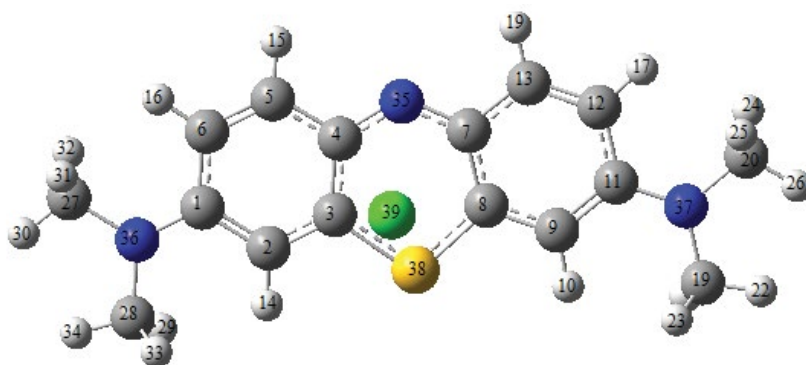


Fig. 1. Chemical structure of methylene blue (MB).

The electronic chemical potential (Eq. (7)) can be calculated from the molecular orbital energies and $E_{\text{HOMO}}/E_{\text{LUMO}}$ borders as follows.

$$\mu = \frac{E_{\text{LUMO}} + E_{\text{HOMO}}}{2} \quad (7)$$

Furthermore, the electrophilic character ω is a reactivity descriptor allowing a quantitative classification of the electrophilic nature of a compound within a relative scale. We proposed ω as a measure of the lowering of the maximum energy due to electron flows between the donor and the acceptor, as shown in Eq. (8).

$$\omega = \frac{\mu^2}{2} \times S \quad (8)$$

The number of transferred electrons (Eq. (9)) was calculated according to the quantum chemical method by the following equation.

$$\Delta N = \frac{-(\chi_{\text{metal}} - \chi_{\text{molecule}})}{2(\eta_{\text{metal}} - \eta_{\text{molecule}})} \quad (9)$$

2.1.2. Molecular modeling and dynamics simulations

The MCDS study was adopted to compute the low configuration adsorption energy for adsorbate/substrate systems. MCDS methodology [18] using adsorption locator code [19,20] implemented in Accelrys Materials Studio version 8.0 (Biovia–Dassaultsystemes) [21]. The simulation was performed with the anatase surface in a simulation box ($35 \times 35 \times 35 \text{ \AA}^3$) with periodic boundary conditions. A vacuum plate of 35 \AA was introduced on the anatase (110) surface and was then enlarged to a $(6 \times 6 \times 6)$ super cell. The TiO_2 (110) crystal surface was selected for this simulation because this is the most stable surface. For the whole simulation procedure, the universal force field was used to optimize the structures of all components of the interest system. Moreover, each adsorption system also included 400 H_2O molecules to simulate the solvent effects. This computational study aims to find the most stable and low-energy adsorption sites and investigate the preferential adsorption of MB forms on anatase (110) in an aqueous medium.

Adsorption energy denotes as the interaction energy between the isolated molecule and the metal surface is estimated as the difference between the total energy of the complex and the sum of the energies of the isolated molecule and isolated TiO_2 may be evaluated using Eq. (10):

$$E_{\text{ads}} = E_{\text{surface/molecule}} - (E_{\text{surface}} + E_{\text{molecule}}) \quad (10)$$

where E_{molecule} , E_{surface} and $E_{\text{molecule-surface}}$ represents the potential energy of a molecule, a clean slab (surface) and the whole system with the molecule adsorbed on the slab, respectively. For the case of explicit the solution, the adsorption energy (Eq. (11)) is calculated by [22–24]:

$$E_{\text{ads}} = E_{\text{surface/molecule/solution}} - (E_{\text{surface/solution}} + E_{\text{molecule/solution}}) + E_{\text{solution}} \quad (11)$$

where $E_{\text{molecule/solution}}$, $E_{\text{surface/solution}}$ and E_{solution} represent the potential energy of a molecule in solution, a slab (surface) in solution and just the solution, respectively.

According to this definition, negative adsorption energy corresponds to stable adsorption on the surface. Negative E_{ads} corresponds to an exothermic process and a larger absolute value of adsorption energy indicates stronger interaction between the surface and the molecule.

2.2. Results and discussion

2.2.1. DFT calculations

2.2.1.1. Electronic distribution

The chemical reactivity of an adsorbed molecule with solid surfaces is studied by a series of quantum-chemical parameters, such as the electron distribution, in order to obtain global information on the localization of electrons, by evaluating the molecular electrostatic potential (MEP), the molecular HOMO and LUMO [25]. MEP analysis has been used to find the reactive sites of the compound. The result below is obtained by DFT optimization. The optimized geometric structures, as well as frontier molecular orbital distributions for neutral and protonated forms of MB, are shown in Fig. 2.

The results show that the HOMO's and LUMO's of the protonated at $\text{N}_{35}\text{N}_{36}$, $\text{N}_{35}\text{N}_{37}$ and $\text{N}_{36}\text{N}_{35}\text{N}_{37}$ are strongly

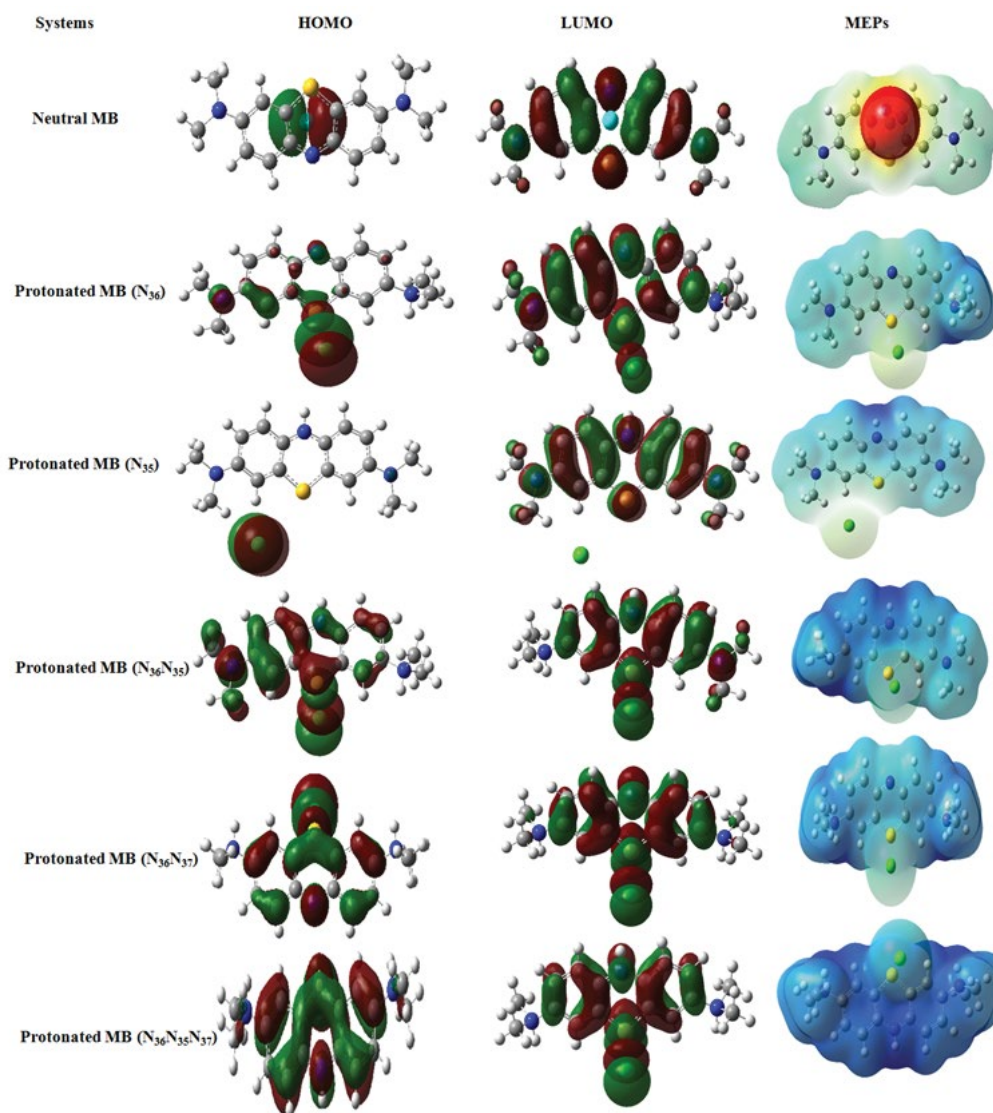


Fig. 2. HOMO, LUMO, and total distribution of electronic density of charge for the protonated and non-protonated species of MB.

delocalized in the aromatic rings and all N atoms. The contour plots of the HOMO and LUMO are structural dependent and the electron density of the HOMO location in the molecule under study is mostly distributed on the atoms having a delocalized character showing that these atoms are the favorite adsorption sites. Note that the strongest contribution for the HOMO is encountered for the N₃₅, N₃₆, and N₃₇ atoms in MB protonated at these atoms. This suggests that the prospective active orbitals for donor-acceptor interactions are distributed over the molecule of the MB protonated at all N, making them capable to donate electrons to the TiO₂-surface, in their chemical adsorption. The LUMOs showed more π -characters than the HOMOs, though surface reflects essentially π -orbitals. The neutral and protonated HOMO of MB in N₃₅ shows the electron density contributed from a chlorine atom, while the LUMO indicates a predominant contribution of the aromatic rings. Some C-atoms of the terminal benzene rings in MB protonated (N₃₆) are also not involved in the HOMO, as the HOMO electron

density is more concentrated around the molecule center. The mono-protonation of the studied MB molecule in the N₃₅ and N₃₆ makes them less reactive, by losing their abundance of electrons, in consequence, the HOMO and LUMO density contour decrease around the active site. The MEPs contour indicates that the reactivity of the MB after protonation decrease because the red color disappears around the active site.

2.2.1.2. Molecular electrostatic potentials

The electronic cloud surfaces, also known as MEPs are electronic cloud surfaces of the molecules. The type of reactivity in a compound was represented using this model. In that case, MEP indicates the color reactivity of the regions for being nucleophilic or electrophilic [26,27].

The MEP of neutral and protonated MB in (N₃₆), (N₃₅), (N₃₆N₃₅), (N₃₆N₃₇), and (N₃₆N₃₅N₃₇) are calculated and mapped on the optimized geometry. They are presented in Fig. 3

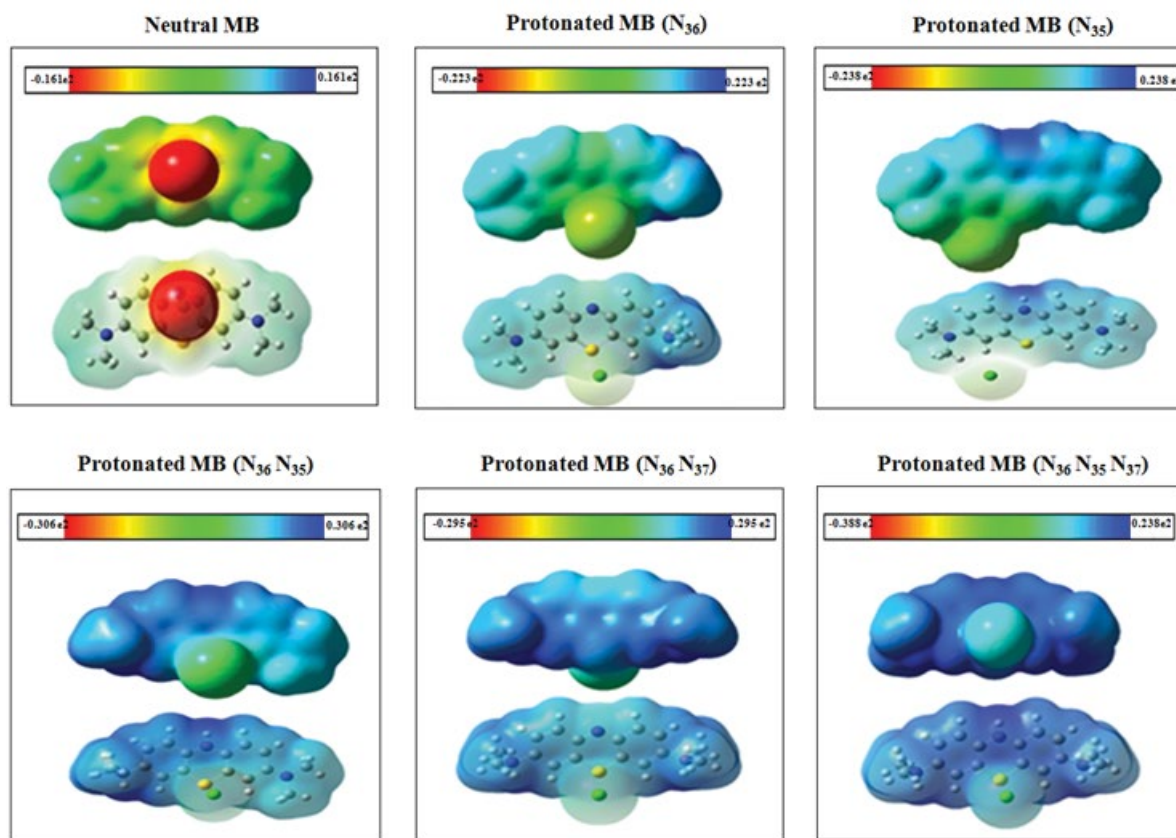


Fig. 3. Molecular electrostatic potential contour map (MEP) for the protonated and non-protonated forms, (Red: Strong negative electrostatic potential (EP); Blue: Strong positive (EP) and Green: Moderately positive (EP).

characteristic increasing values of the electrostatic potential on the surface are indicated by various colors in succession of red (represent electrophilic reactivity) > orange > yellow > green > blue (nucleophilic reactivity). The color code of the MEP diagram lies between -0.388 a.u. (Dark red) and 0.388 a.u. (Dark blue) for MB protonated ($N_{36}N_{35}N_{37}$), -0.295 a.u. (Dark red) and 0.295 a.u. (Dark blue) for MB protonated ($N_{36}N_{37}$), -0.306 a.u. (Dark red) and 0.306 a.u. (Dark blue) for MB protonated ($N_{36}N_{35}$), -0.238 a.u. (Dark red) and 0.238 a.u. (Dark blue) for MB protonated (N_{35}), -0.223 a.u. (Dark red) and 0.223 a.u. (Dark blue) for MB protonated (N_{36}), and -0.161 a.u. (dark red) and 0.161 a.u. (dark blue) for MB neutral. The deep dark blue region around nitrogen atoms of protonated MB molecule represents their nucleophilic nature (electrophilic attack locale), who negatively charged. These electron-rich areas would be the preferred sites for adsorption to the TiO_2 surface. Chlorine atom of neutral MB with deep red color is analyzed to be more electrophilic in nature (nucleophilic attack locale).

2.2.1.3. Quantum chemical parameters

Frontier molecular orbit theory (FMOT) has been applied to investigate the chemical reactivity, active sites, and kinetic stability of the molecule. The E_{HOMO} is related to the electron-donating ability of the compound (filled state). A higher value of E_{HOMO} indicates that the molecule has a higher

tendency towards the donation of an electron to appropriate acceptor molecules with low energy and empty molecular orbital (empty state). In that, the difference in energy between these FMOT presents an analytical parameter in resolving and understanding the molecular transport properties.

The chemical reactivity of the MB molecule has been analyzed by the energy of the lowest unoccupied molecular orbital (E_{LUMO}) and the highest occupied molecular orbital (E_{HOMO}) and of the molecules. MB molecule having a higher value of E_{HOMO} exhibits a higher capability of electron donation to the metal surface [28].

Hence, the protonated molecules having higher values of E_{HOMO} facilitate greater adsorption and act as a good adsorbate to the TiO_2 metal surface. It is seen from Table 1, that the E_{HOMO} values increases in the order: neutral MB < protonated MB (N_{36}) < protonated MB (N_{35}) < protonated MB ($N_{36}N_{35}$) < protonated MB ($N_{36}N_{37}$) < protonated MB ($N_{36}N_{35}N_{37}$). This result shows that the ability of electron donation by the molecule is in the order of MB neutral < protonated MB (N_{36}) < protonated MB (N_{35}) < protonated MB ($N_{36}N_{35}$) < protonated MB ($N_{36}N_{37}$) < protonated MB ($N_{36}N_{35}N_{37}$). In addition, it can also be observed that the values of E_{LUMO} decrease in the order of neutral MB > protonated MB (N_{36}) > protonated MB (N_{35}) > protonated MB ($N_{36}N_{35}$) > protonated MB ($N_{36}N_{35}N_{37}$).

As the ΔE value decreases, there is an increase in reactivity, which influences and increases the adsorption ability of the molecules on the surface of metal [28]. Table 1 reveals also

Table 1
Quantum chemical parameters of protonated and no-protonated MB optimized by DFT/B3LYP/LanL2DZ basis set

Dyes	Forms	E_{HOMO}	E_{LUMO}	ΔE_{gap}	χ	η	S	μ	ω	ΔN
Methylene blue	Neutral	-5.524	-3.619	1.905	4.572	0.953	1.049	-4.572	10.970	0.044
	Protonated (N ₃₆)	-5.659	-4.108	1.551	4.883	0.775	1.289	-4.883	15.376	-3.148
	Protonated (N ₃₅)	-5.986	-4.626	1.36	5.306	0.68	1.470	-5.306	20.701	-3.901
	Protonated (N ₃₆ N ₃₅)	-6.395	-4.979	1.416	5.687	0.708	1.412	-5.687	22.840	-4.016
	Protonated (N ₃₆ N ₃₇)	-6.678	-4.677	2.001	5.678	1.000	0.999	-5.678	16.113	-2.837
	Protonated (N ₃₆ N ₃₅ N ₃₇)	-7.728	-5.551	2.177	6.639	1.088	0.918	-6.639	20.249	-3.049

that decreasing trends in ΔE with increasing protonated sites of MB. Furthermore, this phenomenon is illustrated by the fraction of electron transferred (ΔN) capability between the molecules and the metallic surface. For different four forms (protonated), it is observed that all the calculated ΔN values for anatase (110) surface are negative. This result indicates that the electron donation from the protonated molecules to the metal surface is no longer possible. Absolute electronegativity (χ), Global hardness (η), Global softness (S), and global electrophilicity index (ω) are other important parameters to elucidate the adsorption ability of the molecules on anatase surface. To better understand the chemical reactivity of the molecule, we can use the NBO analysis.

2.2.1.4. Protonated affinity

The presence of heteroatom like N, S in the MB molecule suggests their higher tendency of protonated in acidic solution. As we are discussing all the molecule issues in acid solution, investigation of the protonated form of MB molecule has been considered. In order to select the most desirable site of protonated, the optimization of geometry was performed in several desirable sites and the most preferable site of protonated was determined by protonated affinity (PA) at the different active centers [29]. Most of the organic molecules containing the heteroatoms (=N-, -Cl-, -S-) and several bonds in their molecules facilitate adsorption on the surface. For neutral molecule, protonated reaction at a particular donor site can be written as:



M is the neutral molecule and MH^+ is the protonated species of neutral M.

This proton affinity (Eq. (13)) energy is estimated using the equation:

$$PA = E_{\text{protonated}} + E_{\text{H}_2\text{O}} - E_{\text{non-protonated}} - E_{\text{H}_3\text{O}^+} \quad (13)$$

where $E_{\text{protonated}}$ is the energy of protonated MB molecule, $E_{\text{H}_2\text{O}}$ is the energy of water molecule, $E_{\text{non-protonated}}$ is the energy of neutral MB and $E_{\text{H}_3\text{O}^+}$ is the energy of ion hydronium.

The MB is a symmetrical molecule (or admits plane of symmetry) and is protonated molecule in N₃₆ and N₃₅, the same observation was made for the protonated of MB in N₃₆N₃₅ and N₃₇N₃₅. The calculated energies of protonated are presented in Table 2.

The high negative of PA indicates that the sites are more nucleophile, in consequence, more reactive and vice versa, comparing the six forms (neutral and protonated) we found that MB protonated at all N atoms have the high negative PA which indicates their better reactivity than other forms. These results are in agreement with the other quantum chemical parameters and with the experimental data.

2.2.1.5. NBO charge distribution on protonated and neutral MB

Quantum-chemical parameters such as NBO analysis were made to obtain the electronic properties of these structures and the interactions between different parts of the molecule with high accuracy. NBO plays an important role in explaining the chemical reactivity of a reagent. The atomic charges on the atoms are computed by the NBO population via DFT/B3LYP methods with LanL2DZ basis level. The NBO charges are listed in Table 3. The NBO charges of active atoms contribute significantly to the strength of electrostatic interaction of an atom with others. Therefore, the atomic charges are always along with HOMO and LUMO to analyze the chemical reactivity and the interaction of a molecule with the surface. Whereas NBO analysis showed protonated transfer within the selected donor-acceptor depicting large energy of stabilization for the compounds under study. The results show that the positive charges are mainly localized on hydrogen atoms and sulfur atom and the negative charges are localized on chlorine and nitrogen atoms. While the carbon atoms can be found either negative or positive. NBO loads of neutral BM atoms are found to be more negative than MB protonated in N₃₅, N₃₆, N₃₇, and the other forms of MB (protonated).

2.2.1.5.1. Natural bond orbital analysis

The NBO calculations were performed using the NBO 3.1 program implemented in the Gaussian 09 package [30,31] at the DFT/B3LYP method with LanL2DZ level basis set. Concerning the NBO analyses, the stabilization energy (E^2) indicates the direct relationship between the interaction bonding—antibonding orbitals and the intensity of intramolecular charge transfer. These interactions are observed as an increase in electron density of anti-bonding orbital that weakens the respective bonds. The higher the E^2 value, the molecular interaction between electron donors and electron acceptors is more intensive and the greater the extent of conjugation of the entire system [32].

Table 2
Protonated affinity of protonated MB forms optimized by DFT/B3LYP/LanL2DZ basis set

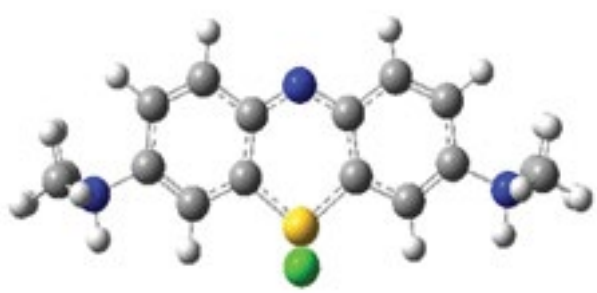
System	Protonated nitrogen	E_{total}	PA (Kcal/mol)
	Protonated MB (N ₃₆)	-22,044.751	-9.425
	Protonated MB (N ₃₅)	-22,045.377	-23.861
	Protonated MB (N ₃₆ N ₃₅)	-22,056.479	-279.884
	Protonated MB (N ₃₆ N ₃₇)	-22,055.962	-267.961
	Protonated MB (N ₃₆ N ₃₅ N ₃₇)	-22,067.581	-22,067.581

Table 3
Calculated NBO atomic charge distribution of neutral and protonated MB using DFT/B3LYP method with LanL2DZ basis set

Atoms	Charges					
	Neutral	Protonated N ₃₆	Protonated N ₃₅	Protonated N ₃₆ N ₃₅	Protonated N ₃₆ N ₃₇	Protonated N ₃₆ N ₃₅ N ₃₇
C1	0.275	0.292	0.281	0.185	0.198	0.188
C2	-0.284	-0.280	-0.239	-0.199	-0.212	-0.184
C3	-0.147	-0.159	-0.159	-0.173	-0.173	-0.177
C4	0.148	0.212	0.224	0.202	0.193	0.242
C5	-0.141	-0.141	-0.176	-0.164	-0.128	-0.168
C6	-0.253	-0.219	-0.200	-0.199	-0.216	-0.165
C7	0.148	0.156	0.203	0.269	0.193	0.242
C8	-0.147	-0.162	-0.153	-0.169	-0.173	-0.177
C9	-0.284	-0.223	-0.255	-0.264	-0.212	-0.184
C11	0.275	0.190	0.277	0.268	0.198	0.188
C12	-0.253	-0.233	-0.209	-0.154	0.216	-0.165
C13	-0.141	-0.129	-0.175	-0.189	-0.128	-0.168
C19	-0.420	-0.392	-0.421	-0.421	-0.392	-0.391
C20	-0.419	-0.392	-0.420	-0.421	-0.392	-0.392
C27	-0.420	-0.420	-0.425	-0.392	-0.392	-0.392
C28	-0.419	-0.421	-0.415	-0.393	-0.392	-0.391
N35	-0.434	-0.362	-0.449	-0.477	-0.440	-0.492
N36	-0.393	-0.437	-0.341	-0.481	-0.483	-0.482
N37	-0.393	-0.481	-0.361	-0.349	-0.482	-0.482
S38	0.415	0.544	0.443	0.654	0.721	0.816
Cl39	-0.986	-0.896	-0.915	-0.626	-0.635	-0.378

Delocalization of electron density between occupied Lewis-type (bond or lone pair) NBO orbitals and formally unoccupied (antibond or Rydberg) non-Lewis NBO orbitals correspond to a stabilizing donor-acceptor interaction [33]. This donor-acceptor interaction can be quantitatively defined in terms of the NBO, which is expressed by second-order perturbation in interaction energy (E^2). For each donor (i) and acceptor (j), the stabilization energy E^2 [34] associated with the delocalization $i \rightarrow j$ is estimated according to Eq. (14):

$$E^2 = \frac{q_i (F_{ij})^2}{(E_j - E_i)} \quad (14)$$

where q_i is the donor orbital occupancy, E_i and E_j are diagonal elements and F_{ij} is the off-diagonal NBO Fock matrix element.

The most forceful and dynamic interactions between the Lewis-type occupied NBO orbital (bonding) with non-Lewis unoccupied NBO orbital (anti-bonding) are calculated, this most important donor-acceptor interaction with high second-order perturbation energies E^2 are provided in Table 4. According to values in the table, the different donors and acceptors indicate that there are just two sorts of donor σ and π and two kinds of acceptor σ^* and π^* . Between these donors and acceptors, observation of perturbation energy E^2 shows the different possible transitions for neutral and protonated MB. The most important electron

transfer is from bonding orbital (BD) of tubes as a donor to anti-bond orbitals (BD*). As can be seen from this table, NBO analysis revealed that the π (C7–C8) \rightarrow π^* (C12–C13) for neutral MB, π (C7–N36) \rightarrow π^* (C3–C4) for protonated MB (N₃₆), π (C3–C4) \rightarrow π^* (C5–C6) for protonated MB (N₃₅), π (C7–C8) \rightarrow π^* (C11–C12) for protonated MB (N₃₆N₃₅), π (C1–C2) \rightarrow π^* (C5–C6) for protonated MB (N₃₆N₃₇), π (C1–C2) \rightarrow π^* (C5–C6) for protonated MB (N₃₆N₃₅N₃₇), interactions give a strong stabilization to the system of the title compound by 65.09, 218.87, 49.70, 61.21, 122.62, and 122.05 kJ/mol, respectively. The results indicate that protonated MB in (N₃₆N₃₅) and (N₃₆N₃₅N₃₇) gives the greatest E^2 values. As illustrated in Table 4, the results of NBO analysis for protonated show that both lone pair (BD) donor orbital on the π (C1–C2) atom interact with the acceptor orbital π^* (C5–C6) of the aromatic ring of protonated MB (N₃₆N₃₇)/(N₃₆N₃₅N₃₇) with a stabilization energy E^2 of 122.62 and 122.05 kcal/mol, respectively. These transitions represent greater contributions from π -electrons having strong intramolecular hyper conjugative interaction.

2.2.2. Molecular dynamic simulation study

MCDS was performed to further study the adsorption behavior of molecules and heavy metals on the anatase (110) TiO₂ surface. Thus, MCDS simulation reasonably predicts the most favorable configuration of the adsorbed neutral and protonated MB forms on the low adsorption energy TiO₂ surface. The Van der Waals, total, electrostatic, average total, and intermolecular energy for the systems under study; TiO₂

Table 4
Stabilization energy E^2 (kcal/mol) of most important donor–acceptor interactions calculated by B3LYP/LanL2DZ basis set for neutral and protonated MB molecule

Donneurs	Accepteurs	E (kcal/mol)					
		Neutral	Protonated N36	Protonated N35	Protonated N36N35	Protonated N36N37	Protonated N36N35N37
$\Pi(\text{C1–C2})$	$\Pi^*(\text{C5–C6})$	17.16	17.14	17.50		122.62	122.05
$\Pi(\text{C1–C2})$	$\Pi^*(\text{C3–C4})$		15.99	17.73			14.62
$\Pi(\text{C3–C4})$	$\Pi^*(\text{C1–C2})$		52.82	40.58	46.59		58.12
$\Pi(\text{C3–C4})$	$\Pi^*(\text{C5–C6})$		62.15	49.67	37.71		48.20
$\Pi(\text{C5–C6})$	$\Pi^*(\text{C3–C4})$		23.28	26.22	18.13		26.75
$\Pi(\text{C5–C6})$	$\Pi^*(\text{C1–C2})$	18.72	18.99	19.32	17.74	17.33	19.15
$\Pi(\text{C7–C8})$	$\Pi^*(\text{C9–C11})$	55.00		40.60	50.39	100.57	58.15
$\Pi(\text{C9–C11})$	$\Pi^*(\text{C7–C8})$	15.79		17.73	26.20	12.51	
$\Pi(\text{C9–C11})$	$\Pi^*(\text{C12–C13})$	17.15	16.89	17.51			
$\Pi(\text{C12–C13})$	$\Pi^*(\text{C9–C11})$	18.74	18.09	19.33			
$\Pi(\text{C12–C13})$	$\Pi^*(\text{C7–C8})$	22.77		26.23	14.38	24.96	26.76
$\Pi(\text{C7–C8})$	$\Pi^*(\text{C12–C13})$	65.09		49.70	61.21	62.85	48.22
$\Pi(\text{C5–C6})$	$\Pi^*(\text{C4–N35})$	26.43				28.60	
$\Pi(\text{C7–N36})$	$\Pi^*(\text{C12–C13})$		68.05				
$\Pi(\text{C7–N36})$	$\Pi^*(\text{C3–C4})$		218.87				
$\Pi(\text{C4–N35})$	$\Pi^*(\text{C5–C6})$	62.81				79.36	
$\Pi(\text{C4–N35})$	$\Pi^*(\text{C7–C8})$	28.52					
$\Pi(\text{C7–C8})$	$\sigma^*(\text{S38–Cl39})$	19.76					
$\sigma(\text{S38–Cl39})$	$\Pi^*(\text{C7–C8})$	23.90					
$\Pi(\text{C3–C4})$	$\sigma^*(\text{S39–Cl40})$		18.16				
$\Pi(\text{C12–C13})$	$\Pi^*(\text{C7–N36})$		26.29				
$\Pi(\text{S39–Cl40})$	$\Pi^*(\text{C3–C4})$		19.70				

(110)/neutral, protonated (N_{36}), protonated (N_{35}), protonated ($N_{36}N_{35}$), protonated ($N_{36}N_{37}$), or protonated ($N_{36}N_{35}N_{37}$) with solvent molecules ($400\text{H}_2\text{O}$) are calculated by optimizing the whole system and presented in Fig. 4. The total energy of configuration m is calculated according to the following sum [35,36]:

$$E_m = E_m^{\text{AA}} + E_m^{\text{AS}} + U_m^{\text{A}} \quad (15)$$

where E_m^{AA} is the intermolecular energy between the MB molecules, E_m^{AS} is the interaction energy between the MB molecules and the TiO_2 (110), and U_m^{AS} is the total intramolecular energy of the MB. The intramolecular energy of the MB forms is not included as its structure is fixed throughout the simulation; therefore, this energy contribution is fixed and vanishes, since only energy differences play a role in adsorption locator calculations.

The total intramolecular energy is the sum of the intramolecular energy of all adsorbates of all components [35,36]:

$$U^{\text{A}} = \sum_{\{N\}_m} U_{\text{intra}} \quad (16)$$

where $\{N\}$ denotes the set of adsorbate loadings of all components in configuration m .

As the simulation starts with a clean TiO_2 (110) adsorbent, the first stage is to adsorb the specified number of water molecules and MB. This is accomplished by a random series of insertion steps and equilibration moves (only moves that do not change the loading are permitted) until the specified loading has been reached. During this stage, only insertion steps that do not create structures with intermolecular close contacts and that pass all adsorbate location constraints are accepted [36].

For neutral and protonated MB adsorption in the presence of water molecules, it is noted that the electrostatic energy is zero; on the other hand, the intramolecular energy is different from 0 kcal/mol but admits a stable energy value. It is also observed that the total energy and the average total energy are positive, which do not exceed 600 kcal/mol, moreover, the energy of van der Waals admits of negative and positive values that do not exceed the values of average total energy. The van der Waals interaction has a dominant contribution to the MB adsorption on the titanium dioxide.

Before performing the Monte Carlo simulation, DFT is applied to systems comprising neutral and protonated MB optimized in the presence of a water solvent molecule. The selected neutral or protonated MB form is placed on the anatase (110) surface, optimized and then run adsorption locator module. Fig. 5 shows the low energy adsorption configurations of the MB (neutral and protonated forms)

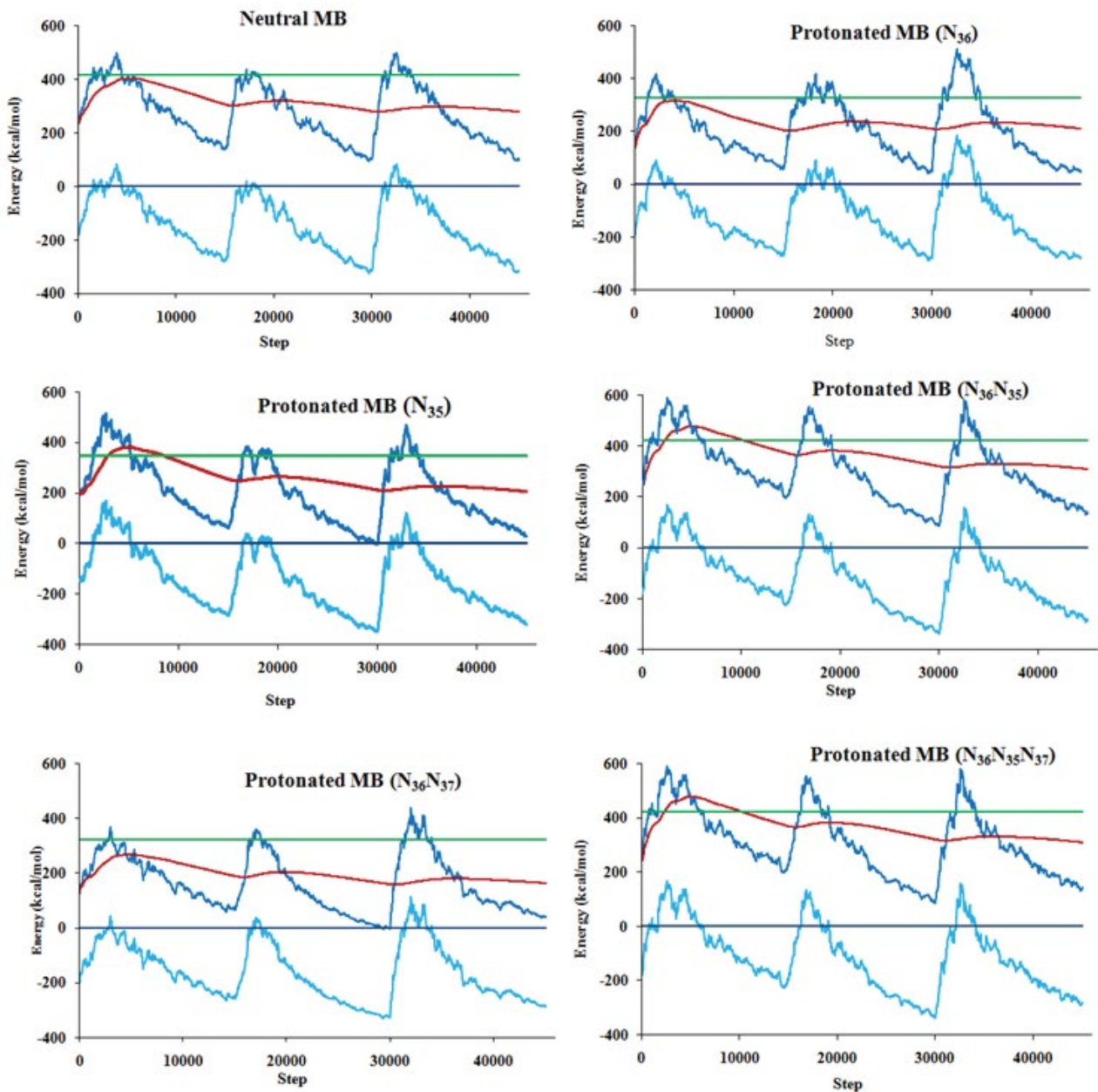


Fig. 4. Total energy distributions for neutral and protonated forms (MB)/400H₂O/TiO₂ (110) obtained by adsorption locator module.

molecules adsorbed onto the anatase (110) surface in the aqueous medium. Side and top views of the most stable adsorption configurations for [neutral and protonated MB/anatase (110)] interfaces are depicted in Fig. 5. The results show that the adsorption centers of MB and its forms (neutral and protonated) on metal oxide surface in the presence of the acid medium are the π -electrons of phenothiazine ring, nitrogen (N), sulfur (S), and chlorine (Cl) heteroatom as well as the possibility of hydrogen bond formation between the molecule and the TiO₂ surface, making it possible to provide electrons to the unoccupied orbitals of TiO₂, to form a stable coordination bonds. From the careful observation of this figure, it can be said that the methylene blue forms

studied adsorb on the titanium dioxide surface in a parallel mode under all circumstances, the adsorbed MB forms also cover a very important part of the TiO₂ surface, indicating that the adsorption capacity for the titanium dioxide studied is reasonable. This is mainly due to the extension of a high protonated effect. According to the quantum-chemical parameters, it is worth noting that the charge density distribution on protonated MB (N₃₆N₃₅N₃₇) is strong than other forms of MB, which enhance the possibility of protonated MB (N₃₆N₃₅N₃₇) to adsorb more strongly on TiO₂ surface than neutral MB and other protonated MB forms. It is confirmed that the more negative the atomic charges of the adsorbed center, the more easily the atom donates its electrons to the

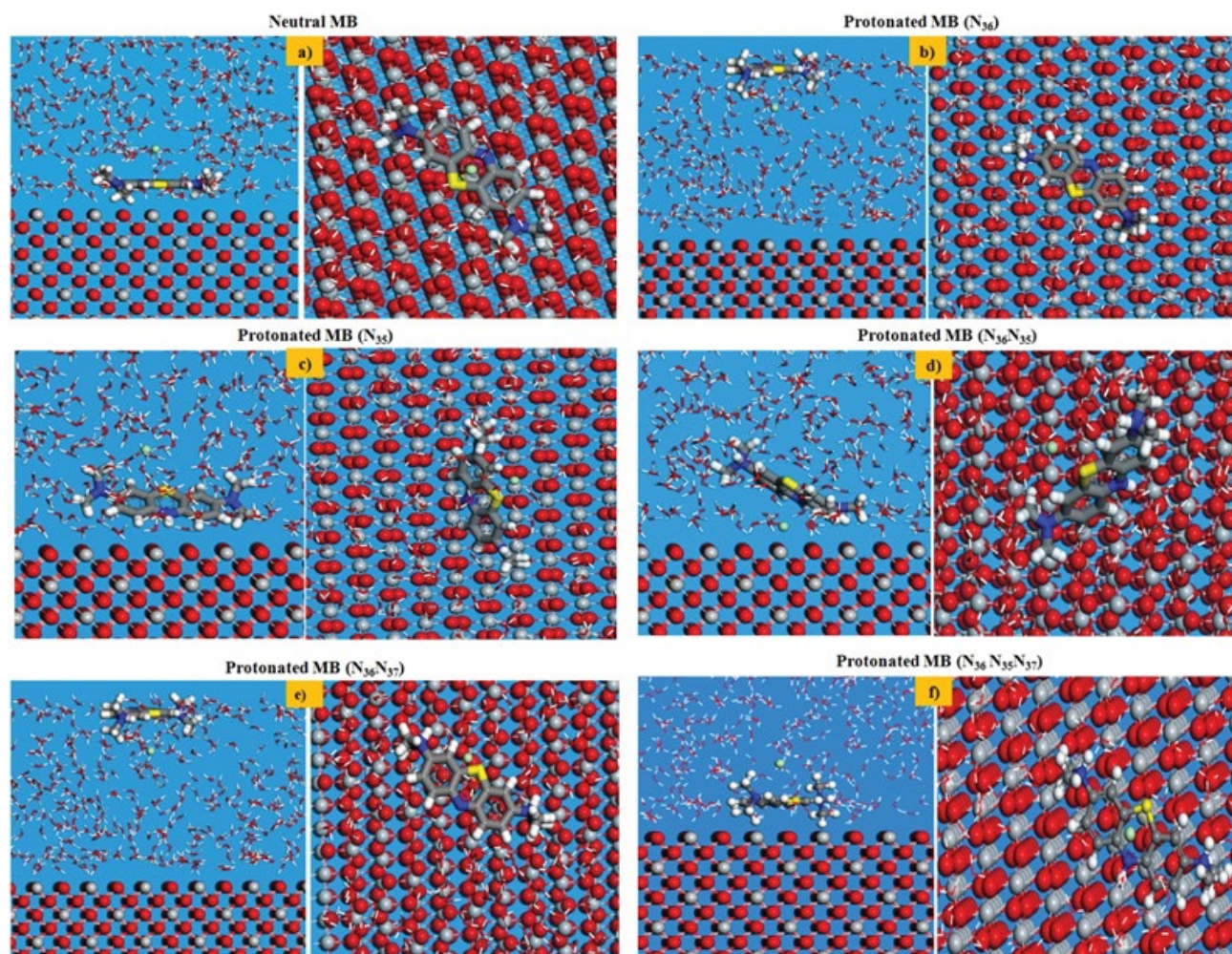


Fig. 5. Side (Left) and top (Right) views of stable adsorption configurations for neutral and protonated forms of MB/400H₂O/anatase (110) TiO₂ interface obtained by adsorption locator module. (a) Neutral MB, (b) protonated MB (N₃₆), (c) protonated MB (N₃₅), (d) protonated MB (N₃₆N₃₅), (e) protonated MB (N₃₆N₃₇), and (f) protonated MB (N₃₆N₃₅N₃₇).

unoccupied orbital of metal dioxide [33]. Therefore, these negative atomic charges indicated that nitrogen, sulfur, and chlorine atoms are the possible active adsorption sites.

The different values of the energies obtained from the adsorption locator module, namely the total energy, the adsorption energy, the rigid adsorption energy, and the deformation energy are collated in Table 5. In addition, ($d_{E_{ads}}/dNi$ (MB forms)) is the energy required to remove an adsorbate from the metal oxide surface, low deformation energy due to adsorbate relaxation on the surface anatase (110) is the most important. The parameters presented in Table 6 include adsorption energy, in kcal/mol⁻¹, of the substrate–adsorbate configuration.

The adsorption energy is defined as the sum of the energies of the adsorbate components, the rigid adsorption energy, and the deformation energy. In addition, adsorption energy reports energy released (or required) when the relaxed adsorbate components (MB forms) are adsorbed on the substrate. As can be seen from Table 5, neutral and protonated MB forms give the maximum adsorption energy in the negative value found during the simulation process.

The high absolute value of the adsorption energy reflects a strong adsorption behavior. Each complex can be characterized by its adsorption energy, E_{ads} , which was calculated from the deformation energy and rigid adsorption energy of the optimized geometries. Indeed, the neutral MB has a low value of the adsorption energy than that of the protonated MB (N₃₆N₃₅N₃₇), indicating that this last form has a high adsorption capacity on the titanium dioxide surface. It is shown from Table 5 that the adsorption energy of neutral, protonated MB (N₃₆N₃₅N₃₇) molecules adsorbed onto the anatase are obtained as -917.155 and -948.456 kcal/mol, respectively, which are much stronger than protonated MB N₃₆, N₃₅, N₃₇, N₃₆N₃₅, and N₃₆N₃₇. This decrease of adsorption energy can be explained by structural modifications in the protonated site (compared to the adsorption of one MB neutral molecule). In parallel with the above, the order of the adsorption energy is confirmed by the efficiency of the selectivity of the reactivity sites obtained from the DFT and the experimental results.

Therefore, the adsorption energy may help us to rank protonated forms of MB. From the result of adsorption

Table 5

Outputs and descriptors calculated by the Monte Carlo simulation for the adsorption of the forms neutral and protonated MB studied on anatase (110) (kcal/mol)

Complex	E_{total}	E_{ads}	RAE	E_{def}	$dE_{\text{ads}}/dNi_{\text{MB}}$	$dE_{\text{ads}}/dNi_{\text{H}_2\text{O}}$
Neutral MB/400 H ₂ O/TiO ₂ (110)	-499.464	-917.155	-556.191	-360.964	-74.178	-1.772
Protonated MB (N ₃₆)/400 H ₂ O/TiO ₂ (110)	-491.175	-819.193	-547.694	-271.498	-72.547	-1.664
Protonated MB (N ₃₅)/400 H ₂ O/TiO ₂ (110)	-484.849	-831.049	-543.333	-287.716	-89.007	-1.710
Protonated MB (N ₃₆ N ₃₅)/400 H ₂ O/TiO ₂ (110)	-487.462	-909.995	-546.815	-363.173	-74.041	-2.096
Protonated MB (N ₃₆ N ₃₇)/400 H ₂ O/TiO ₂ (110)	-490.561	-822.348	-548.679	-273.669	-78.253	-1.542
Protonated MB (N ₃₆ N ₃₅ N ₃₇)/400 H ₂ O/TiO ₂ (110)	-497.154	-948.456	-558.034	-390.421	-111.904	-1.832

Table 6

Parameters of the pseudo-first-order, pseudo-second-order, and Elovich kinetic models together with their regression coefficients for the adsorption of MB

q_{exp}	Pseudo-first-order			Pseudo-second-order			Elovich		
	q_e (mg/g)	k_1 (1/min)	R^2	q_e (mg/g)	k_2 (g/mg min)	R^2	α (mg/g/min)	β (g/mg)	R^2
28.988	27.642	0.531	0.99	28.625	0.043	0.998	1,287,610	0.625	0.942

energy, neutral and protonated MB sites have negative values of adsorption energy suggesting that MB molecule adsorption on anatase (110) TiO₂ surface is exothermic and stable. As well, this result, it is quite clear that the adsorption energies values are negative, which denotes that the adsorption could occur spontaneously [37].

The adsorption energy of the protonated MB (N₃₆N₃₅N₃₇) (-948.456 kcal/mol) is the highest negative value among the MB forms under study, which means that adsorption of this form on titanium dioxide (110) surface in water solvent molecules is stronger than other forms. Furthermore, $dE_{\text{ads}}/dNi_{\text{MB}}$ for protonated MB (N₃₆N₃₅N₃₇) is larger than neutral and protonated, which can say that protonated MB (N₃₆N₃₅N₃₇), it can be said that difficult to remove on the surface of TiO₂. Therefore, these observations are in agreement with experimental results.

So the use of theoretical methods to obtain models that can be used to predict and understand molecular structures, properties, and interactions are known as "Molecular Modeling." This allows providing information that is not available by experience and therefore plays a complementary role to that of experimental chemistry. So to confirm these theoretical results obtained, we performed out the experimental study.

3. Experimental study

3.1. Materials and methods

3.1.1. TiO₂ synthesis

The titanium dioxide was prepared by dissolving the titanium isopropoxide in a solution formed from the methanol-ethanol mixture under stirring with the molar proportion (1:1:10). The solution obtained is maintained at 75°C for 3 h. The solution was hydrolyzed by hot drip in water. After filtering with crucible having a porosity N°4, the solid obtained was dried at 120°C overnight in an oven and calcined at 500°C in a muffle furnace for 4 h.

3.1.2. Adsorption tests

Adsorption experiments were carried out in beakers containing dye solution and continuously stirred 300 rpm for the desired time. A stock solution of dye at 20 mg/L was prepared by dissolving the required mass of the dye in distilled water and subsequent solution concentrations were prepared by suitable dilution. Experiments were done by varying initial concentration from 5 to 20 mg/L, contact time from 5 to 120 min, the mass of TiO₂ from 0.05 to 0.3 g/L, temperature from 25°C to 50°C and solution pH from 2 to 12. The solution pH was adjusted using HNO₃ (0.1 N) and/or NaOH (0.1 N) and was measured by a sensION+ pH meter. At regular intervals, samples were centrifugated and the residual concentration was determined from its UV-vis absorbance characteristic with the calibration curve method at the wavelength of maximum absorption of MB (661 nm). The adsorbed amounts were calculated using the following equation [38,39]:

$$q = \frac{(C_0 - C)V}{m} \quad (17)$$

where q (mg/g) is the adsorbed quantity, C_0 (mg/L) is the initial dye concentration, C (mg/L) is the dye concentration at a time t , V (L) the volume of solution, and m (g) is the mass of adsorbent.

3.2. Results and discussion

3.2.1. Characterization by X-ray diffraction, Fourier transform infrared spectroscopic analysis, Raman spectroscopy, and transmission electron microscopy coupled with energy dispersive X-ray analysis

In order to gain additional insights into the chemical composition of the TiO₂ sample, the X-ray diffraction (XRD)

pattern was recorded from 20° to 80° of 2θ values (Fig. 6a). The figure shows very fine lines, indicating that oxide is well crystallized. As can be seen, TiO_2 sample exhibits practically identical profiles with two very fine peaks corresponding to $2\theta = 25^\circ$ and $2\theta = 30.7^\circ$, which are assigned to reflections from the (101) and (200) planes of anatase structures, it is possible to observe a small shoulder ($2\theta = 30^\circ$) associated to rutile phase formation in TiO_2 nanoparticle (JCPDS file N° 21-1276). The highest intensity of the peak at 2θ equal to 25° results from the anatase phase.

The FT-IR spectra obtained for the TiO_2 sample are shown in Fig. 6b. The figure shows a wideband located between $3,401$ and $1,632\text{ cm}^{-1}$ attributed to the vibrations of elongations of linked hydroxyl groups (O–H) [40]. The second series of bands located in the region $653\text{--}550\text{ cm}^{-1}$ and in the region $495\text{--}436\text{ cm}^{-1}$ are assigned to the deformation modes of the Ti–OH and Ti–O–Ti bonds [41–43]. The band at 640 cm^{-1} is generally attributed to the M–OH bond deformation mode (M, Metal).

Raman spectroscopy is a non-destructive method for studying the vibrational modes of a crystal lattice or molecule. It is widely used for the evaluation of order and disorder structural analysis of titanium dioxide. The Raman spectra obtained for the TiO_2 are shown in Fig. 6c. The five Raman bands observed for the sample heat-treated at 500°C for 5 h. These spectra of TiO_2 exhibit four prominent peaks of 644 , 522 , 403 , and 330 cm^{-1} bands are attributed to the anatase phase of TiO_2 . The band at 251 cm^{-1} is attributed to the rutile phase of titanium dioxide. The results indicate a good agreement with the result found by XRD and Fourier transform infrared spectroscopic (FT-IR) analysis.

To get an idea of the external texture and elemental chemical composition of titanium dioxide, we used elementary transmission mode microscopy coupled with energy dispersive X-ray analysis (EDX). The sample is placed on a circular copper grid with a diameter of 3 mm. this will be covered before performing the analysis with a thin carbon film to facilitate the observation of non-metallic elements.

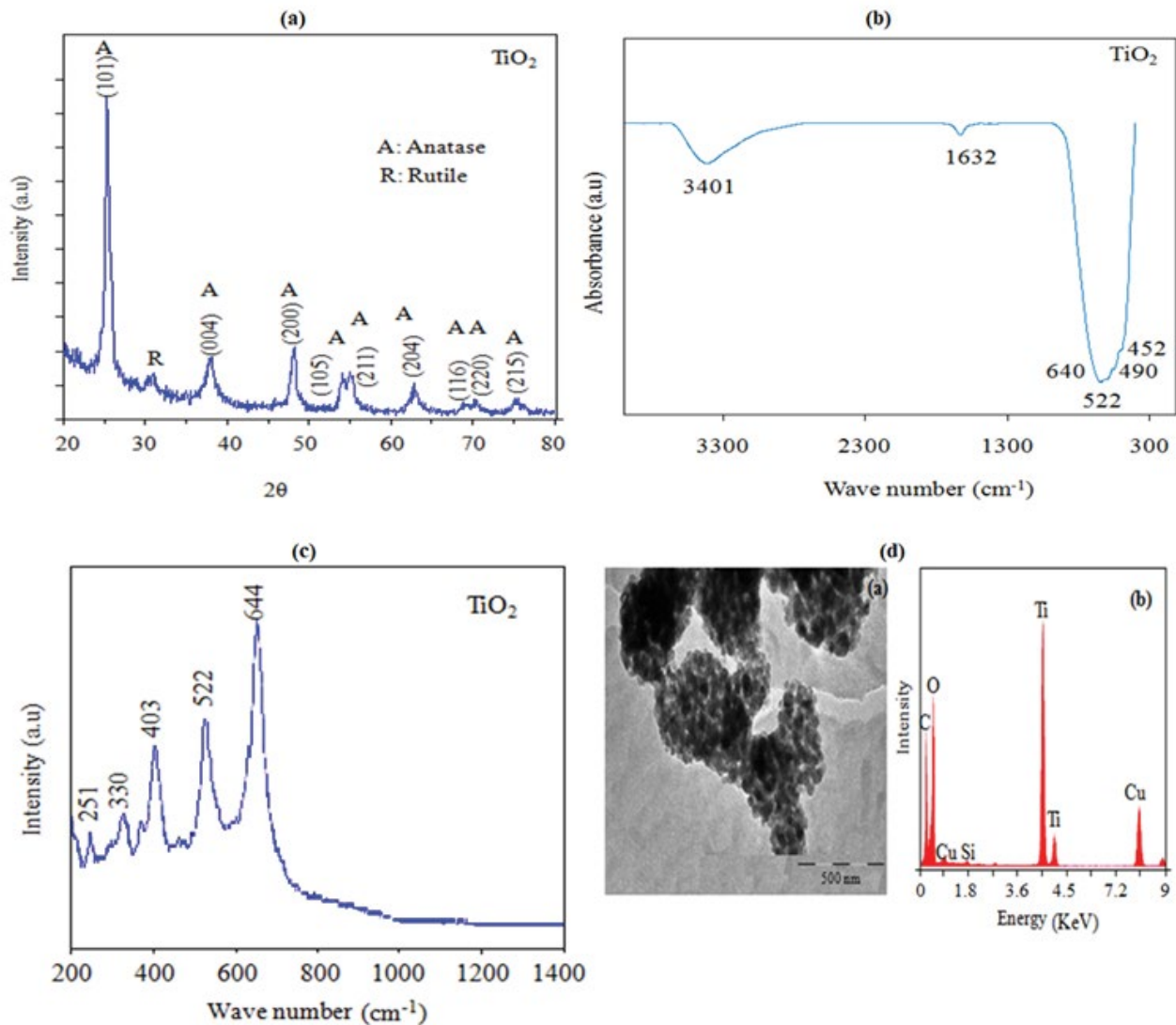


Fig. 6. (a) X-ray diffraction diagram, (b) FT-IR absorption spectrum, (c) Raman spectrum of TiO_2 powder calcined at 500°C , and (d) Transmission electron microscopy image and EDX elementary composition of TiO_2 .

In transmission mode, we see all the particles of our sample located at a sufficiently small thickness to be transparent to electrons. The atomic percentage of the elements is determined, either statistically on several points, or locally on a single zone. Generally, during the analysis, the cooling is provided by zone in the liquid state and zone that better represents our sample is chosen.

The morphological observation of titanium dioxide obtained by elementary transmission mode microscopy coupled to EDX is reported in Fig. 6d. The image shows the morphology of the TiO_2 surface. The solid formed a regular distribution of grains of nanometric size.

EDX analysis was presented in Fig. 6d. The EDX analysis of the TiO_2 surface reveals the presence of the following elements: C, O, Cu, Si, and Ti. The energy peaks 4.5 and 5 KeV correspond to titanium. Also, the energy peaks 0.9 and 8.1 KeV correspond to copper (Cu). The characteristic peaks of the carbon and the copper are due to the dispersion grid of the sample. While titanium represents the majority product present on the surface of solid.

3.2.2. Study of methylene blue adsorption

3.2.2.1. Effect of adsorbent dosage

Fig. 7 illustrates the effect of adsorbent dosage on the adsorption of MB. The figure indicates that the adsorption yield increased from 21.37% to 36.43% for MB when the adsorbent dosage was increased from 0.05 to 0.3 g/L. The result indicates that the adsorption capacity decrease with the increase of TiO_2 dosage. The amount of dye molecule in contact with a unit weight of titanium dioxide decreases with an increase in adsorbent dosage. From a practical view point, the optimum dosage of 0.1 g/L was chosen in further experiments.

3.2.2.2. Effect of pH on the removal of dye

The pH of aqueous solutions is an important parameter that controls the surface chemistry of adsorbent and ionic state of dye molecules. Solution pH affects the chemistry of both the organic molecules and the adsorbents [38]. This is a

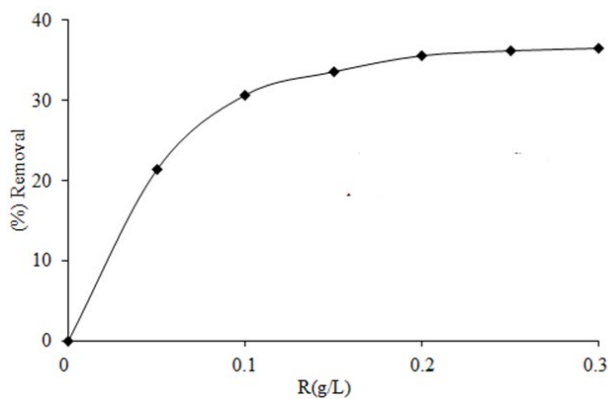


Fig. 7. Effect of adsorbent dosage on the adsorption of MB on TiO_2 : $C_0 = 10$ mg/L, contact time = 180 min, initial pH, and $T = 25^\circ\text{C}$.

factor that characterizes the waters to be treated. The amount of MB adsorbed on TiO_2 as a function of solution pH is presented in Fig. 8. The figure indicates that the amounts of MB removed are higher in the pH range between 2 and 6, but stabilizes with a further increase of pH. There was also an increase in dye adsorption when the solution pH was higher than 8. It appears from these results that the degradation of MB is greater at basic pH. The maximum adsorbed amount of degradation of this dye is observed at pH = 12. The high amount of MB adsorption at pH 12 can be attributed to the electrostatic attraction between the adsorbent and the adsorbate molecule. Under these conditions, the surface of adsorbent has positive charges leading to an electrostatic attraction between MB cationic dye and TiO_2 , which results in increasing the adsorption amount. However, with a decrease, the solution pH, the electrostatic repulsion force between the protons present on the TiO_2 surface and the protonated MB molecule could be the reason for the low adsorption amount at acidic pH. The effect of the initial pH of the solution on the adsorption process is very important because it influences the electrical charge of the particles. The effect of pH on MB adsorption can be interpreted by the term of point of zero charges (pH_{PZC}) of the adsorbent and the pK_a of the MB. The pH_{PZC} of the adsorbents was determined, according to the procedure described by Noh and Schwarz [44]. The point of zero charges of the adsorbent, pH_{PZC} , was determined using the following conditions: 0.1 g TiO_2 and 50 mL 0.01 mol/L NaCl solution. The pH values of the solutions were adjusted with HCl or NaOH to 2, 4, 6, 8, 10, and 12. Samples with and without adsorbent were stirred at 300 rpm for 6 h. ΔpH values were calculated by subtracting the final and initial pH. The pH_{PZC} of the TiO_2 was found to be 7.2 the surface is positively charged for $\text{pH} < 7.2$, and negatively for $\text{pH} > 7.2$. Indeed, according to the zero points of load (pH_{PZC}) of solid, the surface charge of the latter depends on pH. Indeed, in the basic medium, strong adsorption of dye on TiO_2 particles is observed and which is probably due to the electrostatic attraction of TiO_2 negative charge and the positive charge of dye. As can be seen, the maximum adsorption efficiency of dye MB was obtained at pH 12 for TiO_2 adsorbent.

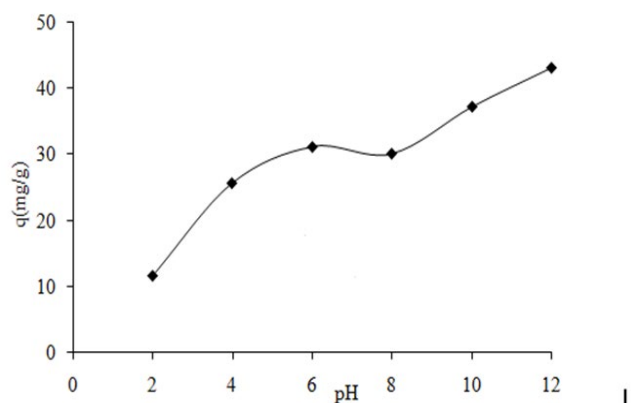


Fig. 8. Effect of pH on the adsorption of MB on TiO_2 : $C_0 = 10$ mg/L, contact time = 180 min, $R = 0.1$ g/L, and $T = 25^\circ\text{C}$.

3.2.2.3. Adsorption kinetics of methylene blue

Kinetics of adsorption is desirable as it provides information about the dynamic of the reaction in terms of order and of the rate constant, which is important for the efficiency of the process. Fig. 9 shows that the adsorbed amount increases with the stirring time to reach until equilibrium is reached after about 60 min. This time indicates that the adsorption balance is reached.

The adsorption amount of the adsorbate during the early minutes of the experiment was much lower than that of the late minutes, meaning that the adsorption capacity of adsorbate increases during the late minutes. This phenomenon may be attributed to the presence of unsaturated active sites on the outer surface of TiO₂. Beyond 120 min, almost no noticeable changes were observed in the adsorption capacity.

Kinetic modeling not only allows estimation of adsorption rates but also leads to suitable rate expressions characteristic of possible reaction mechanisms. Adsorption kinetics data were analyzed using two kinetic models, the pseudo-second-order model [45], the pseudo-first-order model [46], and the Elovich model [47].

The pseudo-second-order model can be expressed as follows:

$$q = \frac{k_2 q_e^2 t}{1 + k_2 q_e t} \tag{18}$$

where k_2 (g/mg min) is the rate constant of pseudo-second-order adsorption.

The first-order rate expression of Lagergren based on solid capacity is generally expressed as follows:

$$q = q_e (1 - e^{-k_1 t}) \tag{19}$$

where q_e and q (both in mg/g) are, respectively, the amounts of dye adsorbed at equilibrium and at any time t (min) and k_1 (1/min) is the rate constant of adsorption.

The Elovich model has been widely used in adsorption kinetics, which describes the chemisorption (chemical reaction) mechanism in nature. This model is suitable for systems with heterogeneous adsorbing surfaces, which is given by Eq. (20):

$$q_t = \frac{1}{\beta} \ln(\alpha \times \beta) + \frac{1}{\beta} \ln(t) \tag{20}$$

where α is the adsorption rate constant (mg/g/min) and β is the desorption rate constant (g/mg).

The obtained data and the correlation coefficients, R^2 are given in Table 6. The table shows that the calculated equilibrium values from the pseudo-second-order model were close to the experimental values than the others calculated from the pseudo-first-order kinetic model. Moreover, the correlation coefficients were closer to 1 in the case of pseudo-second-order than of pseudo-first-order and Elovich models. This result shows that the adsorption of MB onto TiO₂ is better described by the pseudo-second-order model.

Therefore, these observations are in agreement with the experimental results presented in Fig. 9, the equilibrium adsorption capacities (q_e) calculated were slightly more reasonable than those of the pseudo-first-order when compared to the experimental values ($q_{e,exp}$). The MB adsorption process may involve anion exchange, chemical bonding, and electrostatic attraction. For the interpretation of experimental kinetic data, from the point of view, the pedicure of the speed limitation stage is important. So adsorption sites are uniformly energetic the amount adsorbed can be controlled largely by the chemisorption process, in conjunction with the chemical characteristics of titanium dioxide and MB molecule. The distance between the surface and the adsorbed molecule is shorter, which suggests that the adsorption type is a monolayer. These results show that chemical interaction between the blue molecule methylene and the surface of the titanium dioxide by one or more covalent or ionic chemical bonds. The experimental results are in agreement with the theoretical results.

3.2.2.4. Adsorption isotherms

Adsorption isotherms are another important tool that helps in understanding the mechanism of the adsorption process. Also, they provide qualitative information on the capacity of the adsorbent as well as the nature of the solute-surface interaction. Moreover, it gives information about the distribution of the solute between the liquid and solid phases at various equilibrium concentrations. The adsorption isotherms are illustrated in Fig. 10. The figure indicates that as the initial dye concentration increases, the amount adsorbed increases to a limit value corresponding to the maximum amount adsorbed. Also, the shape of the isotherms revealed L-behavior according to Giles et al. [52]. In fact, dye removal is highly concentration-dependent.

Equilibrium data obtained were analyzed using Freundlich, Langmuir, Dubinin–Radushkevich, and Temkin isotherm models. The Freundlich isotherm is an empirical model of heterogeneous surface sorption with non-uniform distribution of heat sorption and affinities [48]. The form of the Freundlich equation can be stated as follows:

$$q_e = K_f C_e^{1/n} \tag{21}$$

where K_f (mg^{1-1/n} g⁻¹ L^{1/n}) is the Freundlich constant and n is the heterogeneity factor. The K_f value is related to

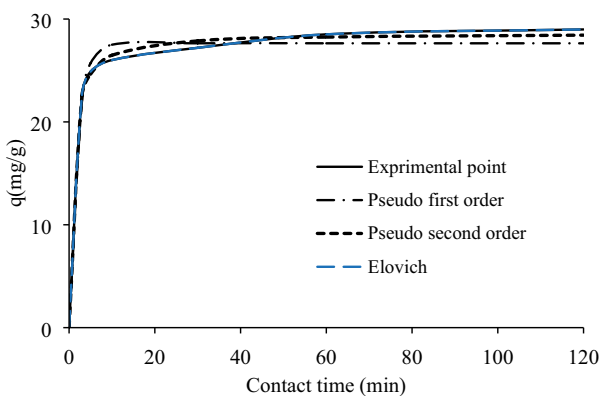


Fig. 9. Kinetics of MB adsorption on TiO₂: $C_0 = 10$ mg/L, $R = 0.1$ g/L, initial pH, and $T = 25^\circ\text{C}$.

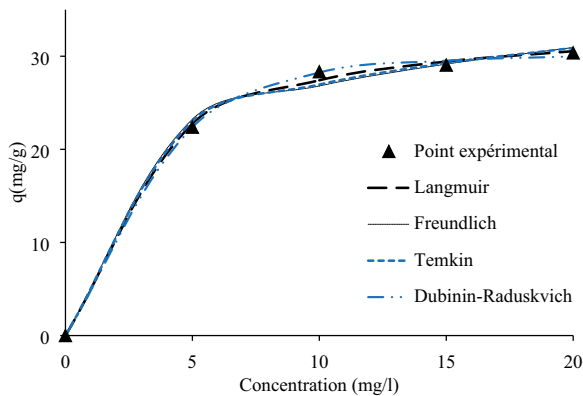


Fig. 10. Isotherms of MB adsorption on TiO_2 : contact time = 180 min, $R = 0.1$ g/L, initial pH, and $T = 25^\circ\text{C}$.

the adsorption capacity; while $1/n$ value is related to the adsorption intensity.

The Langmuir isotherm theory assumes monolayer coverage of adsorbate over a homogeneous adsorbent surface [49]. The Langmuir model is the most frequently used in many sorption processes to evaluate the maximum sorption capacity. The linear form of Langmuir isotherm (Eq. (22)) is represented as follows:

$$q_e = \frac{q_m K_L C_e}{1 + K_L C_e} \quad (22)$$

where q_m (mg/g) is the maximum monolayer adsorption capacity, K_L (L/mg) is the Langmuir equilibrium constant related to the adsorption affinity, and C_e is the equilibrium concentration.

Temkin isotherm model suggests a uniform distribution of binding energies and assumes the effects of the interaction of the adsorbing species and the adsorbate [50]. This isotherm has been expressed mathematically as:

$$q_e = B \ln(K_T C_e) \quad (23)$$

where $B = RT/b$, R is the universal gas constant (8.314 J/mol) and T (K) is the absolute temperature. K_T empirical Temkin constant related to the equilibrium binding constant related to the maximum binding energy (L/mg) and B is the Temkin constant related to the heat of adsorption (kJ/mol).

The Dubinin–Radushkevich isotherm model does not assume a constant sorption potential or a homogenous surface, as other isotherm models do. It can be noted that this isotherm model is more general than the Langmuir model [51]. The Dubinin–Radushkevich model has been written by the following equation:

$$q_e = q_m e^{-\beta \varepsilon^2} \quad (24)$$

where q_m is the theoretical saturation capacity, β is a constant related to the adsorption energy and ε is the Polanyi potential.

The calculated parameters for Freundlich, Langmuir, Dubinin–Radushkevich, and Temkin models are presented

Table 7
Isotherm constants and correlation coefficients for adsorption of MB on TiO_2

Isotherms	Parameters	
Langmuir	q_m (mg/g)	34.473
	K_L (L/mg)	0.388
	R^2	0.998
Freundlich	K_F ($\text{mg}^{1-1/n} \text{g}^{-1} \text{L}^{1/n}$)	16.659
	n	4.839
	R^2	0.995
Temkin	K_T (L/mg)	11.635
	B (kJ/mol)	437.17
	R^2	0.929
Dubinin–Radushkevich	q_m (mg/g)	30.582
	B (mol/J)	0.003
	R^2	0.990

in Table 7. This table shows that the higher values of R^2 accused the applicability of the Langmuir model for MB dye sorption onto the TiO_2 . The adsorption isotherm of MB shows significant adsorption at low concentrations in solution. It is an L-type isotherm in the classification of Giles et al. [52]. The best correlation of the experimental results is obtained with the Langmuir model ($R^2 \sim 0.998$). This result suggests that MB is adsorbed on the surface of titanium dioxide in various ways. Therefore, the Langmuir isotherm assumes that sorption comes from the monolayer coverage of the adsorbate over a homogeneous TiO_2 surface. Generally, this type of adsorption isotherms results from the predominance of strong ionic interactions between the adsorbent and the adsorbate [53–55]. Chemical adsorption of positively charged amine groups of the MB molecule on the negatively charged groups on the surface of the proposed titanium dioxide. The theoretical results also show that the interaction between the MB and TiO_2 surface and chemical type, indicating that these results are probably in accord with the experimental results. The maximum Langmuir adsorption capacity was 34.473 mg/g. These results suggest that the MB adsorption process by TiO_2 is a monolayer.

Maximum adsorption capacity obtained from the removal of MB and onto TiO_2 was compared with the previous records of various low-cost adsorbent as summarized in Table 8. It can be observed that the experimental data of the present study were found to be higher than those of some corresponding adsorbents in the literature.

3.2.2.5. Effect of temperature and thermodynamic parameter

The effect of the increase in the temperature on the adsorption efficiency of MB onto the TiO_2 was studied at various temperatures (i.e., 25°C , 30°C , 40°C , and 50°C) and the results are shown in Fig. 11. The adsorption of MB is less influenced by the temperature, the adsorbed amounts slightly decrease with the increase of solution temperature from 25°C to 50°C . From these results, thermodynamic parameters including the change in free energy (ΔG°), enthalpy (ΔH°), and entropy (ΔS°) were used to describe thermodynamic behavior of the

Table 8
Comparison of maximum adsorption capacity of MB on TiO₂ based on the Langmuir isotherm model should be compared with other studies

Adsorbent	q_m (mg/g)	References
Bagasse	17.54	[55]
Cu ₂ O NPs	2.08	[56]
Natural sand of Morocco	1.185	[7]
Graphene oxide nanosheets (GO) at 25°C	03.57	[7]
Activated lignin–chitosan extruded	36.25	[7]
Kaolinite	102.04	[7]
Raw KT3B kaolin	52.76	[7]
Nanoporous activated carbon	154.8	[7]
TiO ₂	34.473	This study

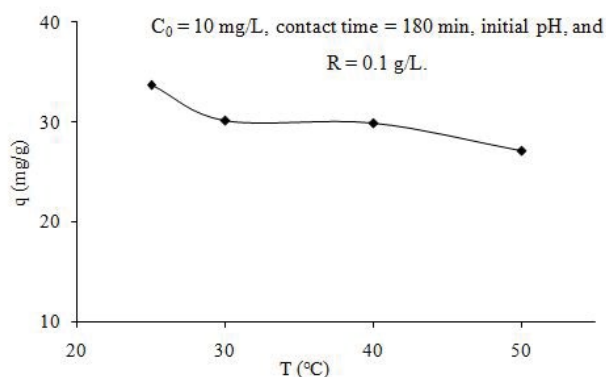


Fig. 11. Effect of temperature on the adsorption of MB onto TiO₂: C₀ = 10 mg/L, contact time = 180 min, initial pH, and R = 0.1 g/L.

adsorption of the dye. These parameters were calculated by considering the following reversible process:



For such equilibrium reactions, K_D , the distribution constant (Eq. (26)), can be expressed as follows:

$$K_D = \frac{q_e}{C_e} \quad (26)$$

The Gibbs free energy is as follows [56]:

$$\Delta G^\circ = -RT \ln(K_D) \quad (27)$$

where G is the universal gas constant (8.314 J/mol/K) and T is solution temperature in K.

ΔH° and ΔS° of adsorption were estimated from the slope and intercept of the plot of $\ln K_D$ vs. $1/T$ yields, respectively [56].

$$\ln K_D = -\frac{\Delta G^\circ}{RT} = -\frac{\Delta H^\circ}{RT} + \frac{\Delta S^\circ}{R} \quad (28)$$

Table 9
Thermodynamic parameters calculated for the adsorption of MB by TiO₂

T (K)	K_D	ΔG° (kJ/mol)	ΔH° (kJ/mol)	ΔS° (KJ/K.mol)
298	1.710	-4.236		
303	1.651	-4.158	-8.917	-0.016
313	1.538	-4.001		
323	1.431	-3.844		

The thermodynamic parameters calculated from the values of the intercepts and the slopes are illustrated in Table 9. The negative values of ΔG° at different temperatures indicate that the adsorption is thermodynamically feasible and is a spontaneous process. The increase in ΔG° values with an increase in temperature from 25°C to 50°C shows a decrease in the feasibility of adsorption at higher temperatures. Also, the magnitude of ΔH° gives information on the type of adsorption, which can be either physical or chemical. The enthalpy of adsorption (ΔH°) was found to be -8.917 kJ/mol. The negative ΔH° is an indicator of the exothermic nature of the adsorption. The ΔS° values were found to be negative which suggests a decreased randomness at the solid-solution interface with the loading of species onto the surface of TiO₂. From all these results, it could be concluded that the adsorption of MB was more favorable by the change in solution temperature.

4. Conclusions

In the present study, the TiO₂ adsorbent was synthesized and structurally characterized by analysis methods such as XRD, FT-IR, Raman spectroscopy, and transmission electron microscopy coupled with EDX, it was prepared in good yield. This adsorbent was successfully synthesized and characterized. Moreover, experimental results show that adsorption was found to be pH-dependent, with strong adsorption of MB (cationic) at high pH. Equilibrium adsorption increases with increasing initial MB concentration in solution. Adsorption isotherms for MB were best fitted with the Langmuir model. The thermodynamic parameters indicated that the adsorption process is exothermic and spontaneous. Our previous experimental results for adsorption of MB on TiO₂ were supported, in the present work, with that obtained by DFT at the B3LYP level and Monte Carlo simulation. Based on the DFT B3LYP/LANL2DZ method, the optimized structures, the electronic parameters, that is, ΔE_{gap} , IE, EA, χ , η , S , ω , ΔN , NBO, and the MEPs are theoretically determined. Hence, the calculated HOMO and LUMO energies showed that charge transfer had occurred within the molecule. MEPs diagram shows that the negative potential sites are in electronegative atoms (denoted as red color) while the positive potential sites are around the hydrogen atoms (denoted as blue color), the small ΔE_{gap} value shows that the molecule has high reactivity. MCDS was further performed to simulate the adsorption of MB neutral and protonated on TiO₂ (110) surface in the presence of molecules of water and the result shows that MB protonated in all

nitrogen atoms has the strongest interaction with TiO₂ surface. Then, the molecular dynamics descriptors show that MB adsorption is chemical and spontaneous. The combination of DFT with MCDS parameters provides an effective means of understanding the interaction mechanism of MB dye with TiO₂. So these results are in agreement with the experimental results, finally, we can conclude that molecular modeling is a method able to predict and understand molecular structures, properties, and interactions mechanisms.

References

- [1] R. Sivaraj, C. Namasivayam, K. Kadirvelu, Orange peel as an adsorbent in the removal of Acid violet 17 (acid dye) from aqueous solutions, *Waste Manage.*, 21 (2001) 105–110.
- [2] S. Agarwal, H. Sadegh, M. Majid, A.S.H. Makhlof, G.A.M. Ali, A.O.H. Memar, R. Shahryari-ghoshekandi, I. Tyagi, V.K. Gupta, Efficient removal of toxic bromothymol blue and methylene blue from wastewater by polyvinyl alcohol, *J. Mol. Liq.*, 218 (2016) 191–197.
- [3] B. Kakavandi, A. Jonidi Jafari, R. Rezaei Kalantary, S. Nasser, A. Esrafil, A. Gholizadeh, A. Azari, Simultaneous adsorption of lead and aniline onto magnetically recoverable carbon: optimization, modeling and mechanism, *J. Chem. Technol. Biotechnol.*, 91 (2016) 3000–3010.
- [4] M. Ahmadi, M. Hazrati, B. Kakavandi, Development of maghemite nanoparticles supported on crosslinked chitosan (γ -Fe₂O₃@CS) as a recoverable mesoporous magnetic composite for effective heavy metals removal, *J. Mol. Liq.*, 248 (2017) 184–196.
- [5] R. Elmoubarki, F.Z. Mahjoubi, H. Tounsadi, J. Moustadraf, M. Abdennouri, A. Zouhri, A. ElAlbani, N. Barka, Adsorption of textile dyes on raw and decanted Moroccan clays: kinetics, equilibrium and thermodynamics., *Water Resour. Ind.*, 9 (2015) 16–29.
- [6] H.H. Abdel Ghafar, G.A.M. Ali, O.A. Fouad, S.A. Makhlof, Enhancement of adsorption efficiency of methylene blue on Co₃O₄/SiO₂ nanocomposite, *Desal. Water Treat.*, 53 (2015) 2980–2989.
- [7] A. Elhalil, M. Barour, H. Tounsadi, R. Elmoubarki, E.M. Lemdek, M. Sadiq, M. Abdennouri, F.Z. Mahjoubi, S. Qourzal, N. Barka, Physicochemical characterization of natural sand from the south-east of Morocco and its potential use as sorbent for dyes removal, *Desal. Water Treat.*, 146 (2019) 362–372.
- [8] M. Kermani, H. Izanloo, R. RezaeiKalantary, H. SalehiBarzaki, B. Kakavand, Study of the performances of low-cost adsorbents extracted from *Rosa damascena* in aqueous solutions decolorization, *Desal. Water Treat.*, 80 (2017) 357–369.
- [9] M. Giahi, D. Pathania, S. Agarwal, G.A. Ali, K.F. Chong, V.K. Gupta, Preparation of Mg-doped TiO₂ nanoparticles for photocatalytic degradation of some organic pollutants, *Stud. Univ. Babeş Bolyai Chem.*, 64 (2019) 7–18.
- [10] M. Abdennouri, A. Elhalil, M. Farnane, H. Tounsadi, F.Z. Mahjoubi, R. Elmoubarki, M. Sadiq, L. Khamar, A. Galadi, M. Baaïala, M. Bensitel, Y. El Hafiane, A. Smith, N. Barka, Photocatalytic degradation of 2,4-D and 2,4-DP herbicides on Pt/TiO₂ nanoparticles, *J. Saudi Chem. Soc.*, 19 (2015) 485–493.
- [11] B. Kakavand, N. Bahari, R.R. Kalantary, E.D. Fard, Enhanced sono-photocatalysis of tetracycline antibiotic using TiO₂ decorated on magnetic activated carbon (MAC@T) coupled with US and UV: a new hybrid system, *Ultrason. Sonochem.*, 55 (2019) 75–85.
- [12] M. Kermani, B. Kakavandi, M. Farzadkia, A. Esrafil, S.F. Jokandan, A. Shahsavani, Catalytic ozonation of high concentrations of catechol over TiO₂@Fe₃O₄ magnetic core-shell nanocatalyst: optimization, toxicity and degradation pathway studies, *J. Cleaner Prod.*, 192 (2018) 597–607.
- [13] T. Tatarchuk, A. Shyichuk, I. Mironyuk, M. Naushad, A review on removal of uranium(VI) ions using titanium dioxide based sorbents, *J. Mol. Liq.*, 293 (2019) 111563
- [14] A.A. Babaei, S.N. Alavi, M. Akbarifar, K. Ahmadi, A.R. Esfahani, B. Kakavandi, Experimental and modeling study on adsorption of cationic methylene blue dye onto mesoporous biochars prepared from agrowaste, *Desal. Water Treat.*, 57 (2016) 1–14.
- [15] M. Gratzel, Photoelectrochemical cells, *Nature*, 414 (2001) 338–344.
- [16] A.G. Thomas, K.L. Syres, Adsorption of Organic Molecules on Rutile TiO₂ and Anatase TiO₂ Single Crystal Surfaces, *Chem. Soc. Rev.*, 41 (2012) 4207–4217.
- [17] M.E. Belghiti, S. Bouazama, S. Echihi, A. Mahsoun, A. Elmelouky, A. Dafali, K.M. Emran, B. Hammouti, M. Tabyaoui, Understanding the adsorption of newly benzylidene-aniline derivatives as a corrosion inhibitor for carbon steel in hydrochloric acid solution: experimental, DFT and molecular dynamic simulation studies, *Arabian J. Chem.*, 13 (2020) 1499–1519. doi: 10.1016/j.arabjc.2017.12.003.
- [18] Y. Karzazi, M.E. Belghiti, F. El-Hajjaji, B. Hammouti, Density functional theory modeling and Monte Carlo simulation assessment of N-substituted quinoxaline derivatives as mild steel corrosion inhibitors in acidic medium, *J. Mater. Environ. Sci.*, 7 (2016) 3916–3929.
- [19] D. Frenkel, B. Smith, *Understanding Molecular Simulation: From Algorithms to Applications*, 2nd ed., Academic Press, San Diego, CA, 2002.
- [20] F. El-Hajjaji, M.E. Belghiti, B. Hammouti, S. Jodeh, O. Hamed, H. Lgaz, R. Salghi, Adsorption and corrosion inhibition effect of 2-mercaptobenzimidazole (Surfactant) on a Carbon steel surface in an acidic medium: experimental and Monte Carlo simulations, *Port. Electrochim. Acta.*, 36 (2018) 197–212.
- [21] Materials Studio Version v8.0, Accelrys Software Inc., San Diego, CA, 2016.
- [22] M.J. Yang, S.L.S. Stipp, J. Harding, Biological control on calcite crystallization by polysaccharides, *Cryst. Growth Des.*, 11 (2008) 4066–4074.
- [23] B.R. Pradip, P. Sathish, Rational design of dispersants by molecular modeling for advanced ceramics processing applications, *KONA Powder Particle J.*, 22 (2004) 151–158.
- [24] H. Zhao, X. Zhang, L. Ji, H. Hud, Q. Let, Quantitative structure-activity relationship model for amino acids as corrosion inhibitors based on the support vector machine and molecular design, *Corros. Sci.*, 83 (2014) 261–271.
- [25] M.E. Belghiti, A. Dafali, I.B. Obot, E.E. Ebenso, K.M. Emran, I. Bahadur, B. Hammouti, F. Bentiss, Anti-corrosive properties of 4-amino-3,5-bis (disubstituted)-1,2,4-triazole derivatives on mild steel corrosion in 2 M H₃PO₄ solution: experimental and theoretical studies, *J. Mol. Liq.*, 216 (2016) 874–886.
- [26] G. Ramesh, B. Venkatram Reddy, Spectroscopic investigation on structure (monomer and dimer), molecular characteristics and comparative study on vibrational analysis of picolinic and isonicotinic acids using experimental and theoretical (DFT & IVP) methods, *J. Mol. Struct.*, 1160 (2018) 271–292.
- [27] M. Khajehzadeh, N. Sadeghi, Molecular structure, X-ray crystallography, spectroscopic characterization, solvent effect, NLO, NBO, FMO analysis of [Cu(bpabza)] complex, *J. Mol. Liq.*, 249 (2018) 281–293.
- [28] N.O. Obi-Egbedi, I.B. Obot, Inhibitive properties, thermodynamic and quantum chemical studies of alloxazine on mild steel corrosion in H₂SO₄, *Corros. Sci.*, 53 (2011) 263–275.
- [29] L.O. Olankanmi, I.B. Obot, M.M. Kabanda, E.E. Ebenso, Some quinoxalin-6-yl derivatives as corrosion inhibitors for mild steel in hydrochloric acid: experimental and theoretical studies, *J. Phys. Chem. C*, 119 (2015) 16004–16019.
- [30] Y.K. Kang, H.S. Park, Assessment of CCSD(T), MP2, DFT-D, CBS-QB3, and G4(MP2) methods for conformational study of alanine and proline dipeptides, *Chem. Phys. Lett.*, 600 (2014) 112–117.
- [31] N.M. O'Boyle, A.L. Tenderholt, K.M. Langner, A library for package independent computational chemistry algorithms, *J. Comput. Chem.*, 29 (2008) 839–845.
- [32] M. Zaboli, H. Raissi, The analysis of electronic structures, adsorption properties, NBO, QAIM and NMR parameters of the adsorbed hydrogen sulfide on various sites of the outer

- surface of aluminum phosphide nanotube: a DFT study, *Struct. Chem.*, 26 (2015) 1059–1075.
- [33] Y. Erdogdu, D. Manimaran, M.T. Güllüolu, M. Amalanathan, I. Hubert Joe, S. Yurdakul, FT-IR, FT-Raman, NMR Spectra and DFT Simulations of 4-(4-Fluoro phenyl)-1H-imidazole1, *Optics Spectrosc.*, 114 (2013) 525–536.
- [34] A. Mahsoun, K. Sadik, M.E. Belghiti, I. Bahadur, A. Aboulmouhajir, Toward a Theoretical understanding of the corrosion inhibitive performance on iron surface by some macrocyclic polyether compounds containing 1, 3, 4-thiadiazole entity, *Int. J. Electrochem. Sci.*, 13 (2018) 8396–8427.
- [35] K.F. Khaled, N.S. Abdelshafi, A.A. Elmaghraby, A. Aouniti, N.A. Almobarak, B. Hammouti, A predictive model for corrosion inhibition of mild steel by thiophene and its derivatives using artificial neural network, *Int. J. Electrochem. Sci.*, 7 (2012) 1045–1059.
- [36] Introduction to Materials Studio, Training Manual, Accelrys Software Inc., San Diego, 2011.
- [37] E.E. Ebenso, M.M. Kabanda, T. Arslan, M. Saracoglu, F. Kandemirli, L.C. Murulana, N. O. Eddy. Quantum chemical investigations on quinoline derivatives as effective corrosion inhibitors for mild steel in acidic medium, *Int. J. Electrochem.*, 7 (2012) 5643–5676.
- [38] F.Z. Mahjoubi, A. Elhalil, R. Elmoubarki, M. Sadiq, A. Khalidi, O. Cherkaoui, N. Barka, Performance of Zn-, Mg- and Ni-Al layered double hydroxides in treating an industrial textile wastewater, *J. Appl. Surf. Interfaces*, 2 (2017) 1–11.
- [39] H. Sadegh, G.A.M. Ali, A.S.H. Makhlof, K.F. Chong, N.S. Alharbi, S. Agarwal, V.K. Gupta, MWCNTs-Fe₃O₄ nanocomposite for Hg(II) high adsorption efficiency, *J. Mol. Liq.*, 258 (2018) 345–353.
- [40] T. Bezrodna, G. Puchkovska, V. Shymanovska, J. Baran, H. Ratajczak, IR-analysis of H-bonded H₂O on the pure TiO₂ surface, *J. Mol. Struct.*, 700 (2004) 175–181.
- [41] Y.F. Chen, C.Y. Lee, M.Y. Yeng, H.T. Chiu, The effect of calcination temperature on the crystallinity of TiO₂ nanopowder, *J. Cryst. Growth*, 247 (2003) 363–370.
- [42] M. Ivanda, S. Musić, S. Porović, M. Gotić, A study of the thermal stability of Fe(IO₃)₃ by 57Fe Mössbauer, FT-IR and Raman spectroscopies, *J. Mol. Struct.*, 480–481 (1999) 645–649.
- [43] K.M.S. Khalil, T. Baird, M.I. Zaki, A.A. El-Samahy, A.M. Awad, Synthesis and characterization of catalytic titanias via hydrolysis of titanium (IV) isopropoxide, *Colloids Surf. A*, 132 (1998) 31–44.
- [44] J.S. Noh, J.A. Schwarz, Estimation of the point of zero charge of simple oxides by mass titration, *J. Colloid Interface Sci.*, 130 (1989) 157–164.
- [45] S. Lagergren, About the theorie of so-called adsorption of soluble substance, *Kungl. Svenska Vetenskapsakad. Handlingar*, 24 (1898) 1–39.
- [46] Y.S. Ho, G. McKay, Pseudo-second order model for sorption processes, *Process Biochem.*, 34 (1999) 451–465.
- [47] A.M. Peers, Elovich adsorption kinetics and the heterogeneous surface, *J. Catal.*, 4 (1965) 499–503.
- [48] H. Freundlich, W. Heller, The adsorption of cis- and trans-azobenzene, *J. Am. Chem. Soc.*, 61 (1939) 2228–2230.
- [49] I. Langmuir, The constitution and fundamental properties of solids and liquids. Part I. Solids, *J. Am. Chem. Soc.*, 38 (1916) 2221–2295.
- [50] Mu. Naushad, S. Vasudevan, G. Sharma, A. Kumar, Z.A. AlOthman, Adsorption kinetics, isotherms, and thermodynamic studies for Hg²⁺ adsorption from aqueous medium using alizarin red-S-loaded amberlite IRA-400 resin, *Desal. Water Treat.*, 57 (2016) 18551–18559.
- [51] F.Z. Mahjoubi, A. Khalidi, M. Abdennouri, N. Barka, M-Al-SO₄ layered double hydroxides (M=Zn, Mg or Ni): synthesis, characterization and textile dyes removal efficiency, *Desal. Water Treat.*, 57 (2016) 21564–21576.
- [52] C.H. Giles, T.H. MacEwan, S.N. Nakhwa, D. Smith, Studies in adsorption. Part XI. A system of classification of solution adsorption isotherms and its use in diagnosis of adsorption mechanisms and in measurement specific surface of solids, *J. Chem. Soc. (Resumed)*, 111 (1960) 3973–3993.
- [53] M. Naushad, Z.A. AlOthman, M.R. Khan, N.J. AlQahtani, I.H. ALSohaimi, Equilibrium, kinetics and thermodynamic studies for the removal of organophosphorus pesticide using Amberlyst-15 resin: quantitative analysis by liquid chromatography–mass spectrometry, *J. Ind. Eng. Chem.*, 20 (2014) 4393–4400.
- [54] F.Z. Mahjoubi, A. Khalidi, M. Abdennouri, N. Barka, Zn–Al layered double hydroxides intercalated with carbonate, nitrate, chloride and sulphate ions: synthesis, characterisation and dye removal properties, *J. Taibah Univ. Sci.*, 11 (2017) 90–100.
- [55] H. Sadegh, G.A.M. Ali, S. Agarwal, V.K. Gupta, Surface modification of MWCNTs with carboxylic-to-amine and their superb adsorption performance, *Int. J. Environ. Res.*, 13 (2019) 523–531.
- [56] G.A.H. Gouda, G.A.M. Ali, T.A. Seaf Elnasr, Stability studies of selected metal ions chelates with 2-(4-amino-1,5-dimethyl-2-phenyl-1,2-dihydro-pyrazol-3-ylideneamino) phenol, *Int. J. Nanomater. Chem.*, 1 (2015) 39–44.